Radiat Environ Biophys (2015) 54:423–431
DOI 10.1007/s00411-015-0612-7

ORIGINAL ARTICLE

Enhanced production of reactive oxygen species by gadolinium oxide nanoparticles under core–inner-shell excitation by proton or monochromatic X-ray irradiation: implication of the contribution from the interatomic de-excitation-mediated nanoradiator effect to dose enhancement

Seung-Jun Seo[1] · Sung-Mi Han[2] · Jae-Hoon Cho[3] · Kazuyuki Hyodo[4] · Alexander Zaboronok[5] · He You[6] · Ken Peach[7] · Mark A. Hill[8] · Jong-Ki Kim[1]

Received: 30 November 2014 / Accepted: 26 July 2015 / Published online: 5 August 2015

Abstract Core–inner-valence ionization of high-Z nanoparticle atomic clusters can de-excite electrons through various interatomic de-excitation processes, thereby leading to the ionization of both directly exposed atoms and adjacent neutral atoms within the nanoparticles, and to an enhancement in photon–electron emission, which is termed the nanoradiator effect. To investigate the nanoradiator-mediated dose enhancement in the radiosensitizing of high-Z nanoparticles, the production of reactive oxygen species (ROS) was measured in a gadolinium oxide nanoparticle (Gd-oxide NP) solution under core–inner-valence excitation of Gd with either 50 keV monochromatic synchrotron X-rays or 45 MeV protons. This measurement was compared with either a radiation-only control or a gadolinium-chelate magnetic resonance imaging contrast agent solution containing equal amounts of gadolinium as the separate atomic species in which Gd–Gd interatomic de-excitations are absent. Ionization excitations followed by ROS measurements were performed on nanoparticle-loaded cells or aqueous solutions. Both photoexcitation and proton impact produced a dose-dependent enhancement in the production of ROS by a range of factors from 1.6 to 1.94 compared with the radiation-only control. Enhanced production of ROS, by a factor of 1.83, was observed from Gd-oxide NP atomic clusters compared with the Gd-chelate molecule, with a Gd concentration of 48 μg/mL in the core-level photon excitation, or by a factor of 1.82 under a Gd concentration of 12 μg/mL for the proton impact at 10 Gy ($p < 0.02$). The enhanced production of ROS in the irradiated nanoparticles suggests the potential for additional therapeutic dose enhancements in radiation treatment via the potent Gd–Gd interatomic de-excitation-driven nanoradiator effect.

Keywords Interatomic de-excitation · Reactive oxygen species · Nanoparticle atomic clusters · Inner-shell ionization · Nanoradiator effect · Low-energy electrons · Radiosensitization

✉ Jong-Ki Kim
jkkim@cu.ac.kr

[1] Biomedical Engineering and Radiology, School of Medicine, Catholic University of Daegu, Daegu, Korea

[2] Anatomy, School of Medicine, Catholic University of Daegu, Daegu, Korea

[3] Neurosurgery, School of Medicine, Catholic University of Daegu, Daegu, Korea

[4] High Energy Accelerator Research Organization (KEK), Photon Factory, Tsukuba, Japan

[5] Department of Neurosurgery, University of Tsukuba, Tsukuba, Ibaraki, Japan

[6] Shanghai Synchrotron Radiation Facility, Shanghai, China

[7] Particle Therapy Cancer Research Institute, University of Oxford, Oxford, UK

[8] Gray Institute for Radiation Oncology and Biology, University of Oxford, Oxford, UK

Introduction

High-Z metal nanoparticles (NPs), including gold (Carter et al. 2007; Hainfeld et al. 2008; Misawa and Takahashi 2011; Polf et al. 2011; Kim et al. 2012), platinum (Porcel et al. 2010), gadolinium (Luchette et al. 2014; Porcel et al. 2014; Miladi et al. 2014; Le Duc et al. 2011) and iron (Kim et al. 2010; Choi et al. 2012), have been actively investigated as novel radiosensitizing agents using either photoexcitation or particle impact. In vivo radiation therapy

experiments exploring the enhancement effect of gold or iron nanoparticles have demonstrated that nanoparticle-loaded mice tumors could be completely eradicated after irradiation with either 250 kVp X-rays (Hainfeld et al. 2004) or protons (Kim et al. 2012; Kim et al. 2010), thereby demonstrating the potential utility of metal nanoparticles for cancer therapy. However, the mechanisms leading to these impressive results have not yet been elucidated. In these studies, it was hypothesized that a larger portion of the energy of the primary ionizing photons was transferred to the tumor due to the increased absorption of X-rays by tumoral gold NPs relative to tissue (Carter et al. 2007; Pradhan et al. 2009), leading to a local increase in the absorbed dose. High-energy protons or carbon ions may transfer energy to high-Z nanoparticles via Coulomb collision with large cross sections relative to tissue atoms (Stolterfoht 1988; Belkić 2010). This energy transfer may enable a highly conformal energy deposition around the NPs, which is caused by a localized spray of escaping photoelectric electrons and X-ray photons or by particle-induced electrons and photons. Extensive theoretical calculations of gold NP doses have been performed using Monte Carlo simulations to explain the observed therapeutic enhancement effect from in vitro and in vivo experiments, despite the absence of a direct quantitative comparison between theoretical and experimental enhancements (Lechtman et al. 2011;Leung et al. 2011; Pradhan et al. 2009; Carter et al. 2007; Cho 2005). However, the theoretical simulations may not fully represent the chemical environments and associated parameters during gold nanoparticle radiosensitization, such as the interaction between the ionized atoms and the neutral atoms inside the irradiated nanoparticles, due to the lack of an appropriate physical model, the intracellular nanoparticle distribution with relative distances to nuclear DNA, the real intracellular or tissue concentration of nanoparticles, the effective radiation energy.

When an atom is electronically excited, it relaxes by emitting a photon or an electron. When embedded in a chemical environment, however, another ultrafast non-radiative decay process, called interatomic/intermolecular Coulombic decay (ICD), can transfer its excess energy to neighboring neutral atoms or molecules and ionize them (Jahnke 2004; Sisourat et al. 2010; Hergenhahn 2012). This interatomic energy transfer generates low-energy ICD electrons very efficiently in atomic/molecular cluster systems that are associated via weak van der Waals interactions or hydrogen bonding (Hergenhahn 2012; Averbukh et al. 2004). This process enhances the production of low-energy electrons compared to separate atomic species (Kim et al. 2011). Because aqueous solutions of nanoparticles produce a typical van der Waals atom–molecule cluster system with a potent hydrogen-bonding hydration layer, various interatomic de-excitations are potentially feasible after the ionization of irradiated atoms, such as interatomic Coulomb decay or interatomic Auger decay (Matthew and Komninos 1975; Kreidi et al. 2008), as illustrated in Fig. 1. Additionally, conventional radiative energy transfer through X-ray fluorescence and Auger decay leads to a cascade of photon–electron emissions in the irradiated

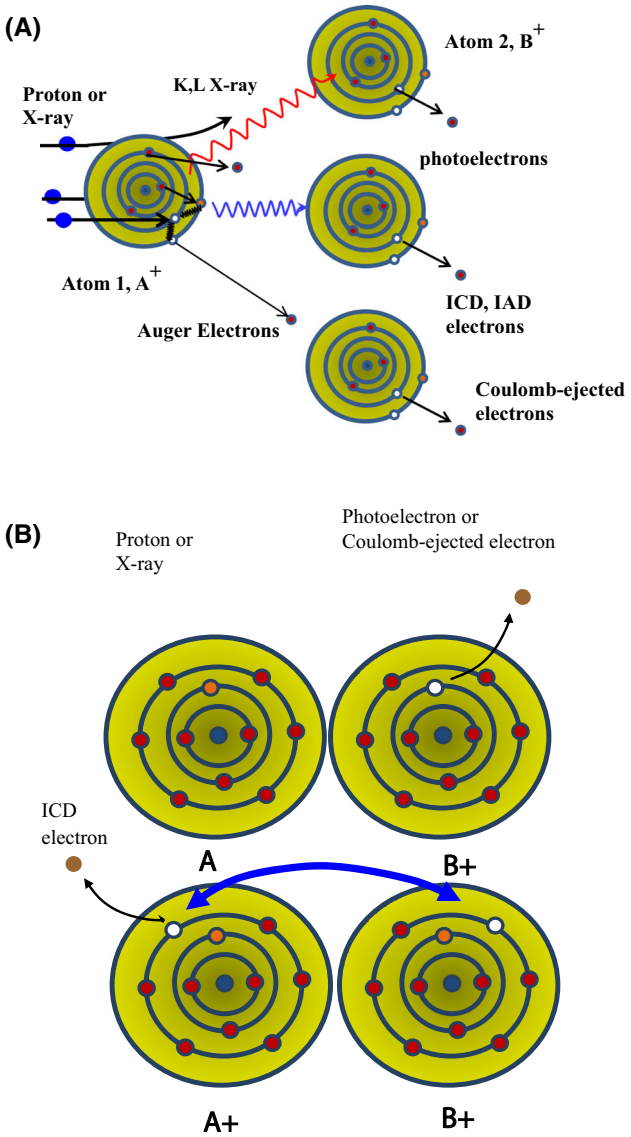

Fig. 1 Schematic diagram describing the potent interatomic relaxation path after core–inner-shell ionization in nanoparticle atomic clusters. Auger decay and characteristic X-ray fluorescence occur in a competitive manner and produce Coulomb-ejected electrons or photoelectrons at adjacent neutral atoms (**a**). However, radiation-less interatomic Coulomb decay (ICD) or interatomic Auger decay (IAD) may occur via the transfer of excess excitation energy to the electrons in a shell of an adjacent neutral atom, generating low-energy electrons on a very fast time scale (**b**). Thus, ionization from neutral atoms that were not impacted by either ions or X-ray photons effectively enhances the production of low-energy electrons upon the absorption of a given amount of energy

high-Z atom, which may impinge upon adjacent neutral atoms within nanoparticles. Thus, we termed the potent interatomic de-excitation-driven enhancement in photon and electron emission from the core–inner-valence ionized nanoparticles using either X-ray photon- or ion-impact the nanoradiator effect.

When nanoradiator occurs in aqueous nanoparticle solutions, the emission of X-ray photons and electrons from the nanoparticle surface may create more radicals via additional water radiolysis compared with a nanoparticle-free solution or a solution of separate atomic species (Carter et al. 2007). Because either photons or charged particles produce core–inner-shell ionization, the present study tests the nanoradiator hypothesis by measuring the apparent ROS yield in gadolinium oxide nanoparticle (Gd-oxide NP) solutions (used as an atomic cluster system, Gd–Gd interatomic de-excitation-present) from the core–inner-shell ionization excitation of Gd with either 50 keV of monochromatic synchrotron X-rays or a 45 MeV proton beam. The ROS yield was compared with a Gd-based MRI contrast agent solution (GdCA) (used as a separate atomic species, Gd–Gd interatomic de-excitation-absent) that contained equal amounts of gadolinium with Gd-oxide NPs. Importantly, enhanced production of ROS was observed from Gd–Gd interatomic de-excitation-present nanoparticle compared with Gd–Gd interatomic de-excitation-absent separate atomic species, exhibiting the potential therapeutic dose enhancements in radiation treatment via the nanoradiator effect. More interestingly, this concept of nanoradiator may suggest better efficiency of radiation detector or solar cell when it is designed by nanoparticle assembly.

Materials and methods

Nanoparticles

Gd-oxide NPs were prepared following a previously reported method (Le Duc et al. 2011). Briefly, gadolinium nitrite salt (4 g, $GdNO_3 \cdot 6H_2O$) was placed in 44 mL of diethylene glycol and completely dissolved at 60 °C under vigorous stirring. When the solution turned clear, a solution of sodium hydroxide (440 mg in 1 mL of water) was added dropwise at 100 °C under vigorous stirring. Then, the solution was heated and stirred at 140 °C for 1 h, following by additional heating and stirring at 172 °C for 4 h. A transparent colloid of Gd-oxide NPs was obtained, which could be stored at room temperature for weeks without changes. A diethylene glycol solution (54 mL) was mixed with 6 mL of a gadolinium nanoparticle solution, heated to 40 °C and stirred for 1 h after adding 0.936 mL of tetraethyl orthosilicate, $Si(OC_2H_5)_4$. A reaction was initiated at 40 °C upon adding the solution to 1.584 mL of a triethylamine solution (0.11 mL of triethylamine in 1.8 mL of distilled water) for 1 h. $Gd_2O_3@SiO_2$ was obtained by precipitating with acetone and centrifuging. The average particle size and the size distribution of the nanoparticles were determined using a 902 transmission electron microscope (Carl Zeiss Pty Ltd, Oberkochen, Germany).

Intracellular nanoparticle concentration and weight percent of gadolinium compound

The cellular uptake of Gd-oxide nanoparticles was measured as a function of the incubating concentration (0, 0.2, 1.0, and 2.0 mg/mL) using an inductively coupled plasma (ICP-MS) mass spectrometer (Thermo Jarrell Ash ARISAP, USA). A total of 5×10^6 CT26 cells were plated in separate Petri dishes containing different concentrations of the nanoparticle solution. The measured data are presented as the average uptake density per 10^6 cells in each incubating dose after harvesting the cells for the ICP-MS measurements. The data are represented as $\mu g/1 \times 10^6$ cells.

The weight percent of gadolinium was measured in solutions of either Gd-oxide NPs or a gadolinium-based MRI contrast agent (Gadovist, Schering AG, Germany; GdCA). From a given stock solution of either Gd-oxide NPs (100 mg/mL) or GdCA (104 mg/mL), a 300-μL aliquot of each was taken to measure the Gd content using ICP-MS.

Measurements of ROS due to the nanoradiator effect

Aqueous solutions of either a gadolinium MRI contrast agent or Gd-oxide NPs containing 9.6, 48, and 96 μg of gadolinium were prepared in 1-mL plastic containers to measure the ROS produced from the X-ray photon-excited nanoradiator effect. One hundred micromolar dihydrorhodamine (DHR) was added to each gadolinium solution. The measurements of the intracellular ROS were performed as previously described (Baluchamy et al. 2010; Mohan et al. 2007) to demonstrate the ROS-mediated dose enhancements in a cellular environment. Briefly, equal amounts of mouse CT26 cells (10^4 cells/well) were seeded in 96-well plates and grown for 24 h. The cells were incubated with 0, 0.2, 1.0, or 2.0 mg/mL Gd-oxide NP solution overnight, washed with phosphate-buffered saline to remove the Gd-oxide NPs that were not taken up by the cells, incubated again with 100 μM DHR for 3 h, and washed again to remove DHR that was not taken up by the cells. Finally, the cells were exposed to different doses of 50 keV synchrotron X-rays at the AR beam line of the Photon Factory (Tsukuba, Japan) (PF) or the Shanghai Synchrotron Radiation Facility (Shanghai, China) (SSRF). The fluorescence resulting from the oxidation of DHR to rhodamine by the

ROS was measured at excitation and emission wavelengths of 485 and 525 nm, respectively, using a fluorescence plate reader (Mithras® LB 940 Multimode reader, Berthold Technologies, Germany). Therefore, the net fluorescence intensity of the oxidized DHR with the irradiated nanoparticles compared with the radiation alone may represent the apparent amount of ROS generated from the nanoradiator-driven secondary radiation, including low-energy electrons. The fluorescence intensities of each sample were measured 3–6 h after irradiation, depending on the distance between the synchrotron/proton accelerator facilities and the measuring sites. Dry ice was used to freeze the samples immediately after irradiation and during transport. The containers of samples were sealed with para film during irradiation, and kept sealed until the measurement of fluorescence.

Core–shell excitation of nanoparticle atoms by monochromatic X-ray irradiation

Core-level excitation was performed for the gadolinium compounds using 50 keV monochromatic synchrotron X-rays at either the PF or the SSRF. The outgoing beam from the monochromator–collimator crystal (Si 111) produced monochromatic and almost plane-parallel X-rays, whose beam size was approximately 35 mm (width) × 4 mm (length) at the PF or 10 mm (width) × 2.5 mm (length) at the SSRF at 50 keV, and the beam was incident to the sample for photoexcitation.

An ionization chamber (T6576, National Institute of Metrology, P. R. China) was used to measure the dose rate. The resulting dose rates were 0.0726 Gy/s at the PF and 0.0383 Gy/s at the SSRF. The irradiation period was controlled for 41 or 138 s at the PF and for 79 or 261 s at the SSRF such that the incident X-ray doses were 3.0 and 10 Gy, respectively. The energy adsorbed by 1 mL of water in a test tube was calculated from the dose rate measured using the ionization chamber.

Photoelectric absorption (PEA) measurement

The radiation dose absorbed via PEA was measured for water solution phantoms of either Gd-oxide nanoparticles or Gadovist containing 10.56 or 21.12 mg of Gd that were irradiated with two different doses (10 and 20 Gy) of 50 keV synchrotron X-rays at the Pohang Accelerator Laboratory. Five different batches of each compound were irradiated, and the absorption measurements were averaged. The 50 keV X-rays were extracted using a double-crystal monochromator with a calibrated radiation dose rate of 0.068 Gy/s. A Gafchromic®HD-810 radiochromic film was attached to either side of the phantom, where the incident and transmitted doses were measured to calculate the dose absorbed by the phantom. A relatively large amount of the gadolinium compound was used to demonstrate the clear difference in the PEA of the two compounds.

The measurement of ROS due to the proton impact nanoradiator effect

Proton impact was performed on a series of water-filled phantoms (inner diameter × length; 6.3 mm × 5 mm) containing gadolinium compounds (either Gd-oxide nanoparticles or gadolinium MRI contrast agent, 12 μg Gd/mL) and 100 μM of DHR using a 45-MeV proton beam at the Korea Cancer Center Hospital (Seoul, Korea). The phantoms were exposed to different doses (0–15 Gy) of traversing protons at the sample position without depositing Bragg peak energy inside the sample, followed by measuring the fluorescence of rhodamine. To maximize the energy transfer portion via nanoradiator with respect to the direct absorption via proton impact inside the solution phantom, the Bragg peak energy was placed outside the phantom. The position of the BP energy was determined by measuring the depth-dose distribution using a water phantom and a waterproofed Markus ion chamber detector that recorded accumulated charges in 1 mm intervals. Dosimetry at the actual sample position and the BP energy outside the sample were determined by measuring the radiation dose with a pair of range shifters and a Gafchromic®HD-810 radiochromic film or a Markus ion chamber (TM34045, PTW, Germany).

Statistical analysis

The nanoradiator effect was evaluated by measuring the ROS produced by each X-ray photon, proton impact nanoparticle solution, or nanoparticle-loaded cell, and was compared with the ROS yield from the X-ray or particle irradiation alone. The difference among the groups was assessed using one-way ANOVA followed by Student's *t* test. A value of $p < 0.05$ was considered to be the level of significance for all tests. All data were analyzed using a contemporary statistical software package (GraphPad Prism™; GraphPad Software, Inc., San Diego, CA, USA).

Results

Nanoparticles and weight percent of gadolinium compound

TEM experiments confirmed that the diameter of the Gd-oxide NPs embedded in a polysiloxane shell did not exceed 45 nm. The arrows in Fig. 2 indicate isolated particles where the dense Gd_2O_3 core appears darker than the lighter

surrounding polysiloxane shell despite the difficulty in clearly visualizing the core–shell structure. The average core diameter of the Gd-oxide NPs was 42 ± 3 nm, and the thickness of the polysiloxane shell was less than 5 nm.

The weight percent of gadolinium was approximately 24.3 % in Gadovist, which contains gadolinium and butrol (macrocyclic dihydroxy-hydroxymethylpropyl-tetraazacyclododecane-triacetic acid), and it was 13.2 % in the gadolinium nanoparticles.

Photoelectric absorption measurement

The absorption of X-rays by the phantom at 50 keV increased with the concentration of gadolinium and the X-ray radiation dose. The results are summarized in Fig. 3. The photoelectric absorption % in the GdCA was enhanced 15 % compared to that in the Gd-oxide nanoparticles.

Comparison of ROS production for the Gd-oxide NPs and the Gd-chelate molecules

ROS production was measured using X-ray photon-irradiated gadolinium solutions of either a gadolinium MRI contrast agent (Gadovist) or gadolinium nanoparticles. The results are presented in Fig. 4. The fluorescence intensity, which represents the apparent ROS yield, increased with the amount of gadolinium and with the X-ray dose compared with the X-rays alone. Observed fluorescence at 0 Gy represents the fluorescence of oxidized DHR from residual oxygen in aqueous solution as observed also in another study of oxidant-based ROS detection (Misawa and Takahashi 2011, Nanomedicine). The ROS enhancement factors of [ROS_{GdNP}/ROS_{GdCA}] or X-ray irradiation were 1.16 ± 0.16 and 1.84 ± 0.43 with a gadolinium concentration of 48 μg/mL with radiation doses of 3 and 10 Gy, respectively. The fluorescence intensity upon proton irradiation also increased with the proton dose for both Gd-oxide nanoparticle and GdCA solutions compared with proton irradiation alone. The ROS enhancement factor of [ROS_{GdNP}/ROS_{GdCA}] for proton irradiation was

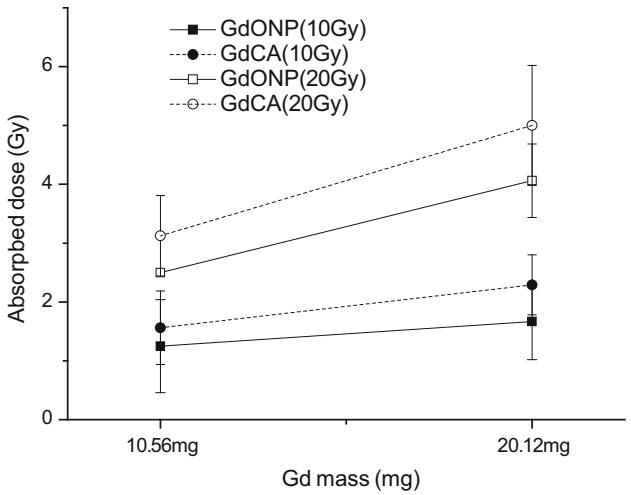

Fig. 3 Absorbed radiation dose of the Gd-oxide NP (GdONp) and Gadovist (GdCA) solutions at the Gd K-line X-ray (50 keV) as a function of two different radiation doses and gadolinium concentrations. Radiation absorption in the GdCA was larger than in the Gd-oxide NPs, typically by 15 %. This PEA-related absorption may lead to direct ionization of gadolinium atoms, the production of photoelectrons, and the subsequent nanoradiator effects during the de-excitation process

1.82 ± 0.17 at 10 Gy with a gadolinium concentration of 12 μg/mL, as shown in Fig. 5. This result suggests that the production of ROS was enhanced in the nanoparticles compared to the separate atomic species with the same amount of gadolinium ($p < 0.02$). With a given radiation dose (10 Gy) and gadolinium concentration, the proton irradiation produced a greater amount of ROS compared with X-ray irradiation because the ROS enhancement factor due to X-ray irradiation (1.84) was achieved with a larger Gd concentration (48 μg/mL) compared with proton irradiation.

Intracellular ROS production due to the nanoradiator effect

The intracellular concentration of Gd-oxide nanoparticles increased as the gadolinium concentration in the incubating

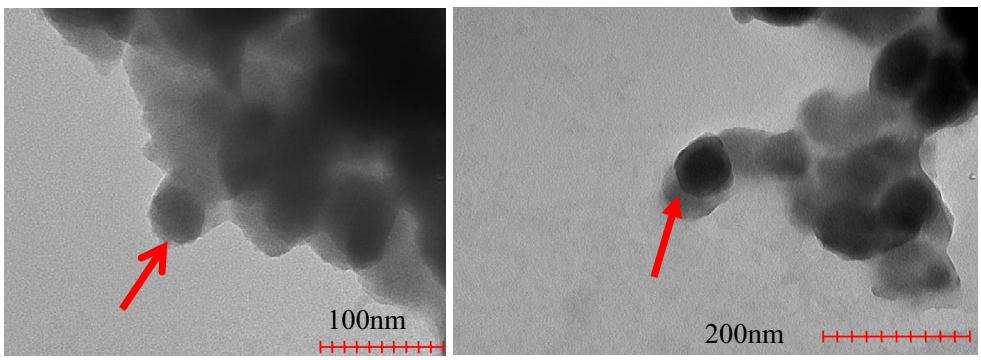

Fig. 2 TEM images of Gd-oxide NPs at two different magnifications ($\times 10^6$ and $\times 5 \times 10^5$). The arrows show that a gray halo is visible around the Gd_2O_3 cores due to the presence of the polysiloxane shell

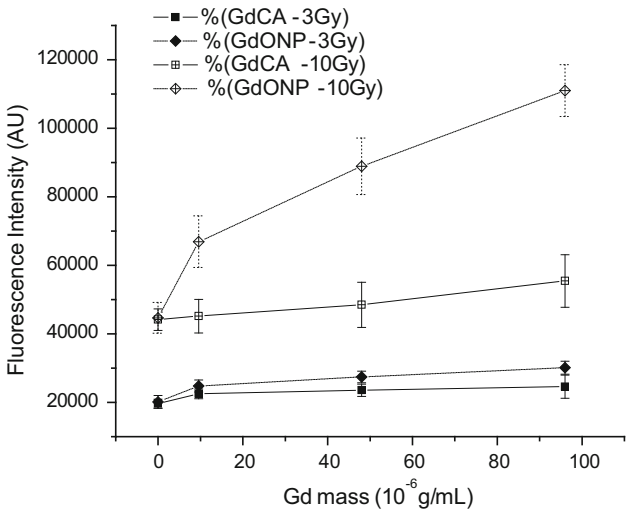

Fig. 4 ROS yields determined from averaged fluorescence measurements of the oxidation of DHR to rhodamine for gadolinium NPs and a gadolinium-chelate molecule (GdCA; Gadovist) solution after core-level excitation of the Gd atoms at two different 50 keV X-ray doses with a given gadolinium concentration

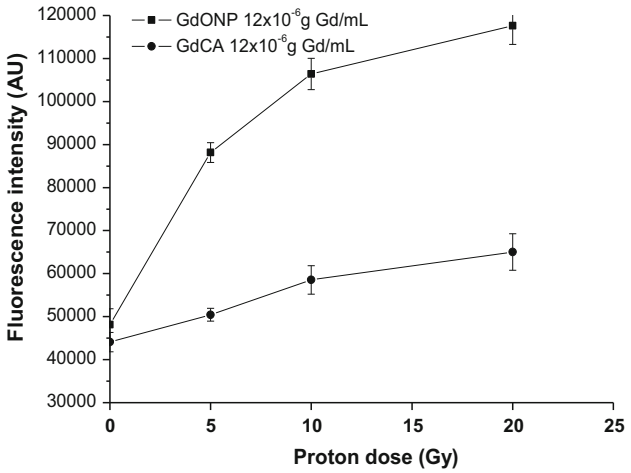

Fig. 5 ROS yields for the same sample sets as in Fig. 2 but after 45 MeV of proton impact on Gd atoms by different proton doses at a gadolinium concentration of 12 μg/mL

solution increased, which is plotted on the x-axis in Fig. 6. The graph in Fig. 6 qualitatively presents the intracellular ROS yields of the ROS-mediated DHR oxidation fluorescence as a function of the intracellular Gd-oxide nanoparticle concentration and compares the yields with the radiation-only control cells at two radiation doses: 3 and 10 Gy. The intracellular ROS increased as the intracellular nanoparticle concentration increased, as shown in Fig. 6. X-ray irradiation of the nanoparticle-loaded cells resulted in more ROS production as a function of dose compared with the X-ray-only control cells. For example, the enhancement factor of the apparent intracellular ROS over

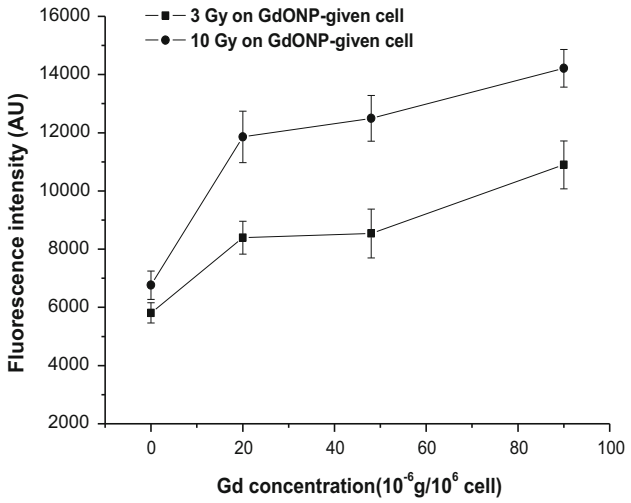

Fig. 6 Intracellular ROS yields determined from averaged fluorescence measurements of the oxidation of DHR to rhodamine after the core–shell excitation of Gd atoms in Gd-oxide NP-loaded CT26 tumor cells by 50 keV. Results are displayed as a function of nanoparticle intracellular concentration at two different X-ray doses (3 and 10 Gy)

the X-ray-only control was either 1.8 ± 0.4 at 3 Gy or 2.6 ± 0.3 at 10 Gy with an intracellular concentration of Gd-oxide NPs of 90 μg/10^6 cells.

Discussion

The IRP-mediated de-excitation after ionization of high-Z atoms in nanoclusters may occur via both Auger electron impact or X-ray fluorescence-mediated radiative energy transfer and non-radiative ICD or IAD, leading to IRP-driven photon–electron emission from the adjacent neutral atoms that were not directly exposed to the X-ray photons or to the ion impact, which effectively changes the irradiation cross section. This concept differs from the conventional PIXE process or photoelectric absorption-mediated Auger decay in which photon–electron emission occurs only at the ionized atom by direct atomic absorption of the radiation. All theoretical works that have calculated the doses in irradiated high-Z nanoparticles had been performed without consideration of interatomic relaxation path in the nanoparticles, resulting in an underestimation of nanoparticle-mediated secondary radiation. We estimate that the relative cross section for the absorption of the X-ray beam by gadolinium atoms between the nanoparticle and separate atomic species solutions would be proportional to the ratio of the molecular size of GdCA to the diameter of Gd-oxide NP and thus be less than 1. With a given amount of Gd, the cross section of Coulomb collision or photoelectric absorption in the nanoparticle solution will be smaller compared with the solution of separate atomic

species due to a screening effect of atomic clustering in nanoparticles (not directly exposed to radiation due to surrounding atoms), resulting in relatively lower photoelectric absorption as shown in Fig. 3. Therefore, the photon–electron emission from the ionized atoms by the direct absorption of radiation resulted in enhanced ROS production in the irradiated nanoparticle solution over the radiation-only control. Additionally, enhanced ROS production was observed in the nanoparticle solution compared with the separate atomic species despite the lower ROS production due to the direct photoelectric absorption effect.

Interatomic/intermolecular Coulombic decay was observed not only at atomic or molecular dimer where they were in van der Waals contact or hydrogen bonding (Jahnke 2015; Hergenhahn 2011) but also between intramolecular atoms like Xe-F in Xenon difluoride (Dunford et al. 2012). Therefore, it is possible to have Gd-N ICD by K-shell ionization in GdCA where Gd atom ligands with four nitrogen atoms. However, the additional electron emission from Gd by Gd–Gd ICD in Gd nanoparticles would exceed the yield from N by Gd-N ICD in molecular gadolinium. The Gd–Gd ICD-mediated electron emission is absent or relatively rare in GdCA compared with Gd-oxide nanoparticles, which is due to the weak non-radiative dipolar coupling between the ionized and the neutral atoms in the separate atomic species that were spread into a considerably larger volume for a given atomic mass. Thus, the present results suggest that the effect of the direct atomic absorption of radiation on the production of ROS was surpassed by the Gd–Gd interatomic de-excitation-mediated production of ROS in the irradiated aqueous nanoparticle solution. This result produces a net ROS enhancement in the Gd-oxide NP solution over the GdCA solution with a given amount of Gd.

The atomic compositions were different for the Gd-oxide nanoparticles and GdCA. Gd-oxide nanoparticles were coated with a molecular layer of Si, O, and H. The light elements other than Gd in both Gd-oxide NP and GdCA are energetically transparent to 50 keV X-rays and may have a smaller collisional cross section with proton beams compared to high-Z Gd, exerting a minimal effect on electron production and the ROS yields. Therefore, the ROS enhancement factor due to the interatomic de-excitation-based difference between the two compounds could be observed via Gd despite the inhomogeneous composition.

In the case of the 50 keV photon excitation of Gd, photon absorption can occur via two main processes: the Compton effect and the photoelectric effect. Compton scattering is only weakly dependent on photon energy and atomic number and consequently becomes the dominant process in low-Z materials, such as soft tissue. During Compton scattering, an incident photon is scattered by a weakly bound outer-shell electron of Gd. The photon loses energy, which is transferred to the electron from the atom that is ejected without an Auger cascade. In contrast, incident 50 keV photons due to the photoelectric effect are completely absorbed by inner-shell electrons that are then ejected from the Gd atom, generating a burst of photon-electron emission via Auger cascades. Thus, photoelectric absorption is the major path for photon interactions with gadolinium nanoparticles to produce nanoradiator and ROS enhancement compared with the Compton effect. The ejected Compton electrons and the formation of electron–hole pairs in the Gd-oxide NP suspension can cause a loss of excess energy, and the Compton electrons can become thermalized with the localization in a trap state within the nanoparticle. Eventually, the two carriers can either recombine near the nanoparticle surface or cross into the aqueous solution, leading to enhanced radiolytic yields (Schatz et al. 1999).

The most significant consequence of decreasing the nanoparticle size is the increase in the surface/volume ratio, thus changing structural factors. Interatomic activation is not limited to surface atoms but can be extended to bulk atoms as a generalized form without difference between ICD and Auger decay due to metallic bonding status. Thus, bulk activation includes intra-NP production of slow electrons via radiation-less cascade despite lower probability of electrons escaping from the internal nanoparticle, as it had been considered from theoretical dose calculation (Carter et al. 2007). Low-energy ICD electrons of 1–10 eV may have a mean free path of 10–100 nm and have sufficient energy to escape from the surface barrier because the coating thickness is less than 5 nm in the Gd-oxide NPs. Low-energy electrons of 0–1 keV escaping from the nanoparticle surface lose their energy by undergoing further ionization and excitation, generating a trail of radical species ($H^{\cdot}$, $^{\cdot}OH$, e^{-}_{aq}, $O_2^{\cdot-}$, and H^{+}_{aq}) along their paths. These radical species subsequently diffuse and react, forming molecular species, including H_2 and H_2O_2, in less than approximately 1 μs; they can alternatively be interconverted by known reactions, e.g., $H_2O_2 + e^{-}_{aq} \rightarrow OH^{-} + {}^{\cdot}OH$ and $H^{\cdot} + H_2O_2 \rightarrow H_2O + {}^{\cdot}OH$. The oxidation of DHR to rhodamine is triggered by several oxidants with different reaction speeds ($^{\cdot}OH$, $O_2^{\cdot-}$, and H_2O_2; a faster reaction in the presence of peroxidase, $^{\cdot}NO_2$, $ONOO^{-}$, ferrous ion, and others) (Kalyanaraman et al. 2012; Qin et al. 2008). Thus, the oxidation of DHR to rhodamine is nonspecific but is conveniently detected by a broad range of oxidizing reactions that may be increased during the nanoradiator process or during intracellular oxidative stress (Kalyanaraman et al. 2012).

The observation of similar ROS enhancement factors between the photon excitation and the proton impact with different amounts of Gd and the same radiation dose

suggests that there is more nanoradiator induction via inner–outer shell ionization by proton impact compared with photon excitation. The 45 MeV proton beam may excite multiple inner valence levels or multiple electrons in an inner shell via Coulombic attraction compared with the single-level ionization by the 50 keV monochromatic synchrotron X-rays, leading to an enhanced production of photon-electrons under a given irradiation condition.

The enhancement of radiation cytotoxicity was reported under either X-ray or ion beam irradiation in a number of previous studies with high-Z nanoparticle-loaded cells. This may be attributed to nanoparticle-mediated dose enhancement or biological interaction with nanoparticles. The claim for biological response needs to address elucidation of the importance of nanoparticle-induced radical production, hypoxia, and cell signaling pathways. Similar-scaled enhancement of ROS production in a water-filled phantom and in intracellular space upon X-ray irradiation suggests a significant contribution of the nanoradiator-mediated dose enhancement effect to radiosensitization, as demonstrated in our preceding report on nanoparticle-loaded tumor cells under proton irradiation (Kim et al. 2012).

Production of additional electron emission from the irradiated high-Z nanoparticles by both radiative and interatomic radiation-less energy transfer may bring up new ideas not only in the dosimetry and theoretical dose simulation of radiation oncology but also in the design of light- or charged particle-receiving nano-devices. These may include a site-specific therapeutic nano-beacon when inert prodrug high-Z nanoparticle is transformed into electron-emitting drug, and a metal-oxide nanoparticle-based radiation detector or a photovoltaic cell with high-yield efficiency.

Conclusions

The production of ROS was enhanced in a nanoparticle solution compared with radiation alone or in a solution of separate atomic species, suggesting a contribution in ROS production from the dose enhancement due to the Gd–Gd interatomic de-excitation-mediated nanoradiator effect. The enhanced production of ROS in either nanoparticle solutions or the nanoparticle-loaded cells suggests a dependence of dose enhancement on the radiosensitization effect of nanoparticles under X-ray photons or proton irradiation. This result may add to the knowledge in the field of nano-device development for radiation detectors or light-harvesting collectors as well as therapeutic nano-beacon.

Acknowledgments The authors greatly thank Prof. Reinhard Dörner at Goethe University, Germany, for the discussion about interatomic Coulomb decay in ionized nanoparticles and its potential relevance to the nanoradiator effect. This work was performed with financial support from the Basic Science Research Program, International Corporation Foundation Establishment Program and Atomic energy research expansion program through the National Research Foundation of Korea funded by the Ministry of Education, Science and Technology (20090088454, 2012M2A7A1026636, 2013M2B2B1075774). This work was also partially supported by research Grants (20115004) from the Catholic University of Daegu in 2012.

References

Averbukh V, Müller IB, Cederbaum LS (2004) Mechanism of interatomic Coulombic decay in clusters. Phys Rev Lett 93:263002–263006

Baluchamy S, Ravichandran P, Periyakaruppan A, Ramesh V, Hall JC, Zhang Y, Jejelowo O, Gridley DS, Wu H, Ramesh GT (2010) Induction of cell death through alteration of oxidants and antioxidants in lung epithelial cells exposed to high energy protons. J Biol Chem 285:24769–26774

Belkić D (2010) Review of theories on ionization in fast ion-atom collisions with prospects for application to hadron therapy. J Math Chem 47:1366–1419

Carter JD, Cheng NN, Qu Y, Suarez GD, Guo T (2007) Nanoscale energy deposition by X-ray absorbing nanostructures. J Phys Chem B 111:11622–11625

Cho SH (2005) Estimation of tumor dose enhancement due to gold nanoparticles during typical radiation treatments: a preliminary Monte Carlo study. Phys Med Biol 50:163–173

Choi G-H, Seo S-J, Kim K-H, Kim H-T, Park S-H, Lim J-H, Kim J-K (2012) Photon activated therapy (PAT) using monochromatic Synchrotron X-rays and iron oxide nanoparticles in a mouse tumor model: feasibility study of PAT for the treatment of superficial malignancy. Radiat Oncol 7:184–194

Dunford RW, Southworth SH, Ray D, Kanter EP, Krässig B, Young L, Arms DA, Dufresne EM, Walko DA, Vendrell O, Son S-K, Snatra R (2012) Evidence for interatomic Coulomb decay in Xe K-shell-vacancy decay of XeF_2. Phys Rev A 86:033401–033412

Hainfeld JF, Slatkin DN, Smilowitz HM (2004) The use of gold nanoparticles to enhance radiotherapy in mice. Phys Med Biol 49:N309–N315

Hainfeld JF, Dilmanian FA, Slatkin DN, Smilowitz HM (2008) Radiotherapy enhancement with gold nanoparticles. J Pharm Pharmacol 60:977–985

Hergenhahn U (2011) Interatomic and intermolecular Coulombic decay: the early years. J Electron Spectrosc Relat Phenom 184:78–90

Hergenhahn U (2012) Production of low kinetic energy electrons and energetic ion pairs by intermolecular Coulombic decay. Int J Radiat Biol 88:871–883

Jahnke T (2004) Experimental observation of interatomic Coulombic decay in neon dimmers. Phys Rev Lett 93:163401–163404

Jahnke T (2015) Interatomic and intermolecular Coulombic decay: the coming of age story. J Phys B 48:082001–082010

Kalyanaraman B, Darley-Usmar V, Davis KJA, Dennery PA, Forman HJ, Grisham MB, Mann GE, Moore K, Jackson Roberts L II, Ischiropoulos H (2012) Measuring reactive oxygen and nitrogen species with fluorescent probes: challenges and limitations. Free Radic Biol Med 52:1–6

Kim J-K, Seo S-J, Kim K-H, Kim K-H, Kim T-J, Chung M-H, Kim K-RK, Yang T-K (2010) Therapeutic application of metallic nanoparticles combined with particle-induced x-ray emission effect. Nanotechnology 21:425102

Kim H-K, Titze J, Schöffler M, Trinter F, Waitz M, Voigtsberger J, Sann H, Meckel M, Stuck C, Lenz U, Odenweller M, Neumann N, Schössler Ullmann-Pfleger K, Ulrich B, Costa Fraga R, Petridis N, Metz D, Jung A, Grisenti R, Czasch A, Jagutzki O, Schmidt L, Jahnke T, Schmidt-Böcking H, Dörner R (2011) Enhanced production of low energy electrons by alpha particle impact. PNAS 108:11821–11824

Kim J-K, Seo S-J, Kim H-T, Kim K-H, Chung M-H, Kim K-R, Ye S-J (2012) Enhanced proton treatment in mouse tumors through proton irradiated nanoradiator effects on metallic nanoparticles. Phys Med Biol 57:8309–8323

Kreidi K, Jahnke T, Weber Th, Havermeier T, Liu X, Morisita Y, Schössler S, Schmidt LPH, Schöffler M, Odenweller M, Neumann N, Foucar L, Titze J, Ulrich B, Sturm F, Stuck C, Wallauer R, Voss S, Lauter I, Kim HK, Rudloff M, Fukuzawa H, Prümper G, Saito N, Ueda K, Czasch A, Jagutzki O, Schmidt-Böcking H, Stoychev S, Demekhin PV, Dörner R (2008) Relaxation processes following 1 s photoionization and Auger decay in Ne_2. Phys Rev A 78:043422–043431

Le Duc G, Miladi I, Alric C, Mowat P, Bräuer-Krisch E, Bouchet A, Khalil E, Billotey C, Janier M, Lux F, Epicier T, Perriat P, Roux S, Tillement O (2011) Toward animage-guided microbeam radiation therapy using gadolinium-based nanoparticles. ACS Nano 5:9566–9574

Lechtman E, Chattopadhyay N, Cai Z, Mashouf S, Reilly R, Pignol JP (2011) Implications on clinical scenario of gold nanoparticle radiosensitization in regards to photon energy, nanoparticle size, concentration and location. Phys Med Biol 56:4631–4647

Leung MKK, Chow JCL, Chithrani BD, Lee MJ, Oms B, Jaffray DA (2011) Irradiation of gold nanoparticles by X-rays: Monte Carlo simulation of dose enhancements and spatial properties of secondary electrons production. Med Phys 38:1–8

Luchette M, Korideck H, Makrigiorgos M, Tillement O, Berbeco R (2014) Radiation dose enhancement of gadolinium-based AGuIX nanoparticles on HeLa cells. Nanomed Nanotechnol Biol Med 10:1751–1755

Matthew JAD, Komninos Y (1975) Transition rates for interatomic auger processes. Surf Sci 53:716–725

Miladi I, Aloy MT, Armandy E, Mowat P, Kryza D, Magné N, Tillement O, Lux F, Billotey C, Janier M, Rodriguez-Lafrasse C (2014) Combining ultrasmall gadolinium-based nanoparticles with photon irradiation overcomes radioresistance of head and neck squamous cell carcinoma. Nanomed Nanotechnol Biol Med. doi:10.1016/j.nano.2014.06.013

Misawa M, Takahashi J (2011) Generation of reactive oxygen species induced by gold nanoparticles under x-ray and UV irradiations. Nanomed Nanotecnol Biol Med 7:604–614

Mohan S, Koyoma K, Thangasamy A, Nakano H, Glickman RD, Mohan N (2007) Low shear stress preferentially enhances IKK activity through selective sources of ROS for persistent activation of NF-B in endothelial cells. Am J Physiol Cell Physiol 292:C362–C371

Polf JC, Bronk LF, Driessen WHP, Arap W, Pasqualini R, Michael Gillin M (2011) Enhanced relative biological effectiveness of proton radiotherapy in tumor cells with internalized gold nanoparticles. Appl Phys Lett 98:193702

Porcel E, Liehn S, Remita H, Usami N, Kobayashi K, Furusawa Y, Le Sech C, Lacombe S (2010) Platinum nanoparticles: a promising material for future cancer therapy? Nanotechnology 21:085103

Porcel E, Tillement O, Lux F, Mowat P, Usami N, Kobayashi K, Furusawa Y, Le Sech C, Li S, Lacombe S (2014) Gadolinium-based nanoparticles to improve the hadrontherapy performances. Nanomed Nanotechnol Biol Med 10:1601–1608

Pradhan AK, Nahar SN, Montenegro M, Yu Y, Zhang HL, Sur C, Mrozik M, Pitzer RM (2009) Resonant X-ray enhancement of the auger effect in high-Z atoms, molecules, and nanoparticles: potential biomedical applications. J Phys Chem A 113:12356–12363

Qin Y, Lu M, Gong X (2008) Dihydrorhodamine 123 is superior to 2,7-dichlorodihydrofluorescein diacetate and dihydrorhodamine 6G in detecting intracellular hydrogen peroxide in tumor cells. Cell Biol Int 32:224–228

Schatz T, Cook AR, Meisel D (1999) Capture of charge carriers at the silica nanoparticle/water interface. J Phys Chem B 103:10209–10213

Sisourat N, Kryzhevoi NV, Kolorenč P, Scheit S, Jahnke T, Cederbaum LS (2010) Ultralong-range energy transfer by interatomic Coulombic decay in an extreme quantum system. Nat Phys 6:508–511

Stolterfoht N (1988) Electronic process in ion-atom collisions. In: Berényi D, Hock G (eds) Lecture notes in physics 294. Springer, Berlin, pp 3–36